Computational Insights into the Alkylation Reactions of Pyridine and Pyridinium Quinone Methide Precursors: Studies Towards the Realkylation of Aged Acetylcholinesterase

Research Thesis

Presented in Partial Fulfillment of the Requirements for graduation *with research distinction* in Chemistry in the undergraduate colleges of The Ohio State University

by

Keegan P. Fitzpatrick

The Ohio State University
December 2013

Project Advisors: Dr. Christopher S. Callam, Dr. Ryan J. Yoder and Dr. Christopher M. Hadad, Department of Chemistry and Biochemistry

Abstract

Acetylcholinesterase (AChE) is an essential enzyme in the human body, which hydrolyzes the neurotransmitter acetylcholine into choline and acetate at neurosynaptic junctions. Organophosphorus (OP) nerve agents such as Sarin, Soman, and Tabun are covalent inhibitors of AChE. Following exposure to OPs, AChE is inhibited and undergoes a subsequent irreversible aging process in which the OP-AChE adduct is de-alkylated, resulting in the accumulation of excess acetylcholine in the central nervous system. Current oxime-based pharmaceuticals can only be used to treat the inhibited AChE and are ineffective on the aged AChE. Our research focuses on re-activation of the aged AChE. Quinone methides (QM) have been shown to react with phosphates to form an O–C bond, and such structures may potentially reverse the damage done to the active site on aged AChE through a kinetically favored alkylation of the phosphylated serine residue in aged AChE. Computational methods were used to analyze the potential reaction pathways and docking poses in AChE of pyridine and pyridinium derived quinone methide precursors (QMPs). A model phosphonate group was created and used to study the S_N1 and S_N2 reaction pathways of the QMP via our computational protocol. The S_N1 pathway was determined to be the most energetically favorable mechanism. Snapshots of an aged AChE were used for our docking calculations where the QMPs were allowed to interact with the enzyme active site. Based on docking studies, the most promising therapeutic QMPs are pyridinium complexes with a methylated nitrogen and the alkyl chain at a meta position relative to the oxygen substituent. Studies of molecular dynamic simulations are in progress.

Acknowledgements

I would like to thank my organic lab and lecture professor, Dr. Adam Keller. Dr. Keller's passion for organic chemistry made me to want to pursue a doctorate degree and become a professor of organic chemistry. His mentoring throughout my undergraduate studies been greatly appreciated.

I would like to thank my research advisors, Dr. Christopher Callam and Dr. Christopher Hadad, for giving me the opportunity to do research in their group; and for their inspiration and support the past year. Their knowledge and motivation has increased my passion for organic chemistry has strengthened and I hope to one day have the same influence on future students.

I would like to thank Dr. Ryan Yoder and Jason Brown for their knowledge and guidance on this research project. I learned a tremendous amount about computational chemistry from them. I have enjoyed learning the topic so much that I want to continue computational-organic chemistry throughout graduate school.

I would like to thank Andrew Franjesevic for being an incredible research partner and allowing me to share his data to help present this thesis.

I would also like to thank the Choose Ohio First scholarship program to help me get through school debt free and reassuring me that I want to pursue a future in a STEMM field. Lastly, I want to thank my family for their undying encouragement and support throughout my undergraduate studies; without them my studies could not have been possible.

Table of Contents

List of Figures

List of Schemes

List of Tables

1. Introduction

1.1 The Use of Quinone Methide Precursors to Reverse the Aging of AChE from Organophosphorus Exposure.

The use of organophosphorus (OP) compounds as chemical warfare agents is a growing concern based on recent terrorist and military activity in the Middle East. The most recent example of using OP compounds as chemical warfare agents occurred during the ongoing civil war in Syria. The Assad government allegedly used sarin gas against its own citizens, killing about 1,400 people, including civilians and children.[1] OP compounds are also used as pesticides by farmers to protect their crops from insects and animals; however, small residues of the toxins remain on the plant and can be ingested by the general population.[2] OP compounds (Figure 1.1) contain a phosphonate or a phosphate group that is known to inhibit the enzyme acetylcholinesterase (AChE) which is essential for regulating biochemical communication in the human body.

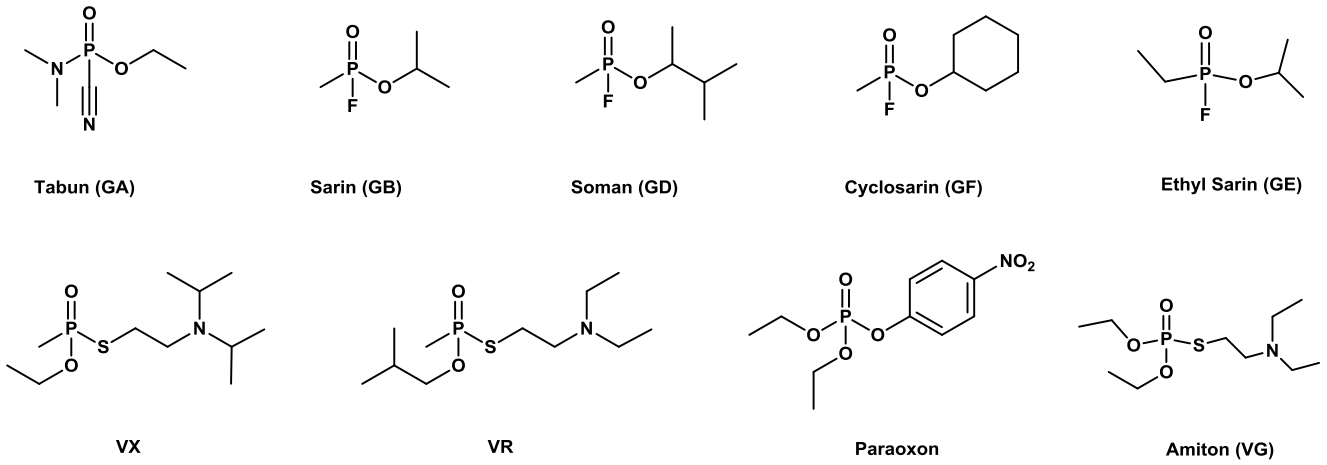

Figure 1.1. OPs used as chemical warfare agents and less toxic pesticides amiton and paraoxon.

AChE is an essential enzyme that hydrolyzes acetylcholine into choline for function in the nervous system. When OP compounds enter the body, they form a covalent bond in the active site of the enzyme at the amino acid Ser-203. This form of the enzyme is called the inhibited form (Scheme 1.1). The inhibited enzyme then undergoes an irreversible aging process (Scheme 1.1) in which the

newly formed chemical species undergoes a dealkylation, thereby leaving a stable methylphosphonate (or phosphate) anion in the active site. Aging of the inhibited enzyme can occur within a few minutes to hours depending on the OP; inactivation of the AChE enzyme from its normal function eventually leads to an excess of acetylcholine at the neurosynaptic junctions. The accumulation of excess acetylcholine results in overstimulation and disruption of neurotransmitters in the central nervous system. There are many negative side effects of OP poisoning and buildup of acetylcholine ranging from vomiting, respiratory issues, kidney failure, and ultimately death.[2] Currently, there are only certain oxime pharmaceuticals available that can reverse the effects of the inhibited AChE, but none are effective against the fully aged AChE enzyme.

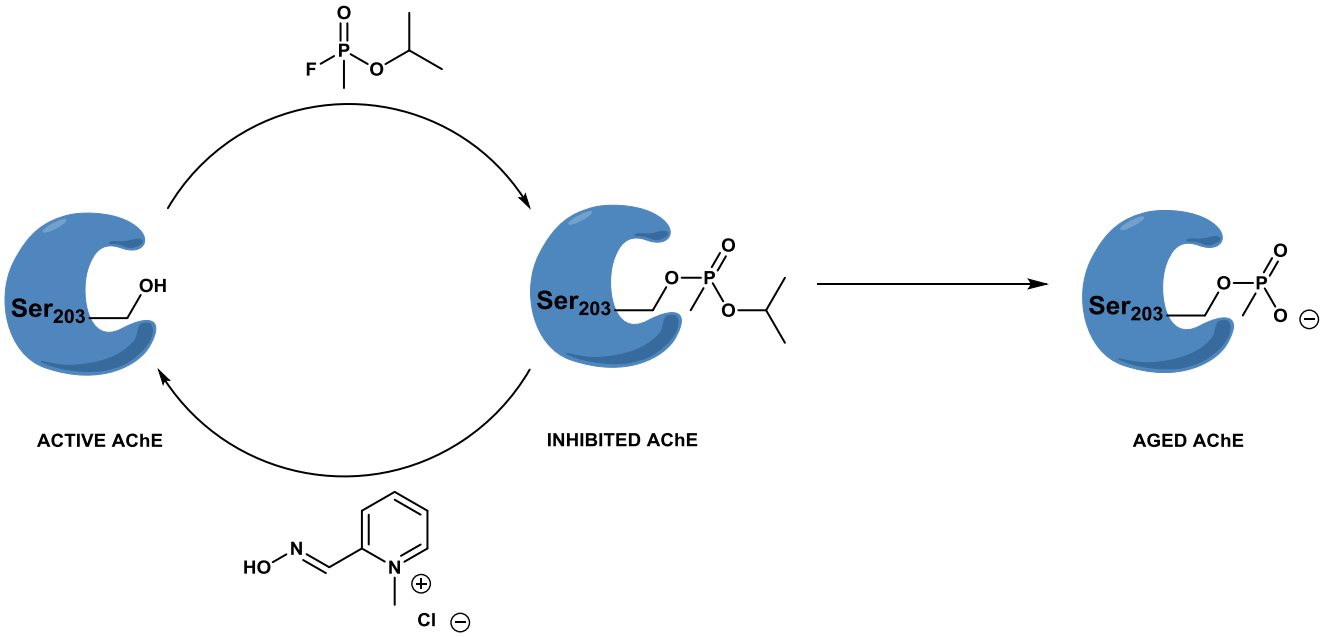

Scheme 1.1. Irreversible aging process of AChE where an alkyl group "R" is lost from the OP adduct.

Current research has been devoted to synthesize compounds that have the potential to re-alkylate the aged AChE-OP adduct. For our study, the compounds of interest were high energy quinone methides (QMs) because of their electrophilic character and previous uses in important biological processes such as lignin biosynthesis in plants, cross-linking of structural proteins, and DNA

alkylation.[3,4] A previous study from Modica et al. determined that these QMs had the ability to alkylate various nucleophiles, specifically amino acids. A key step in the alkylation of the nucleophile was the formation of the *o*-QM intermediate from a quinone methide precursor (QMP). The formation of *o*-QMs and their reactivity with a nucleophile were studied under physiological conditions via thermal and photochemical methods (Scheme 1.2).[5]

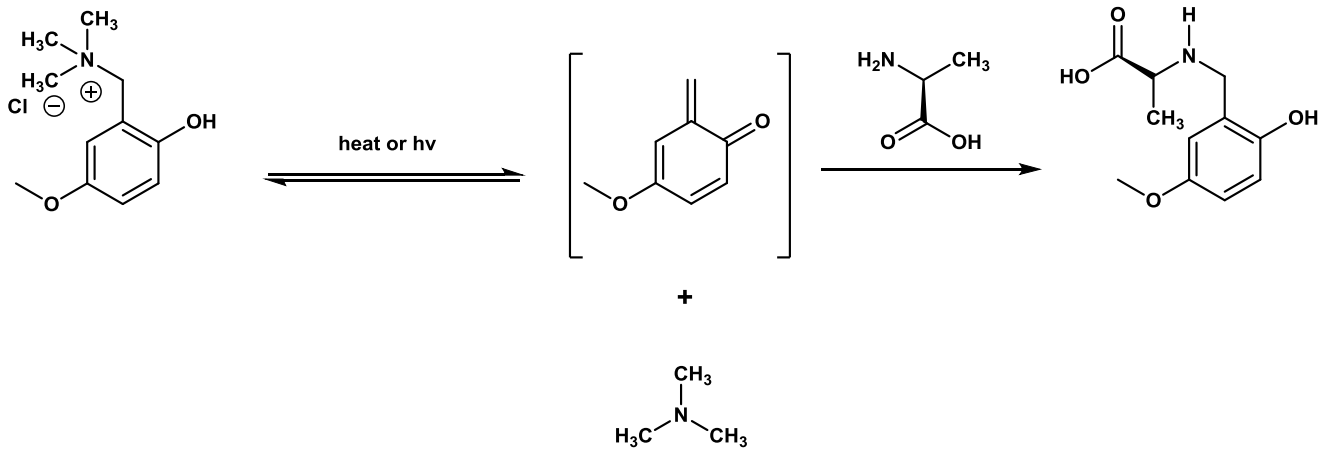

Scheme 1.2 Formation of the *o*-QM to alkylate an amino acid nucleophile.

Another study from Bakke et al. reported that QMs have the ability to re-alkylate a phosphodiester under aqueous conditions, and this study in particular is the motivation for some of this research. The QMs were formed in this experiment via oxidation reactions with lead (II) oxide and silver (I) oxide from *para* oriented QMPs.[6] The ability of these QMs to re-alkylate a phosphodiester (Scheme 1.3) is advantageous to the current research because the OP compounds that inhibit AChE form a phosphodiester bond with Ser-203 before the aging process occurs. These findings suggest the hypothesis that *para* and *ortho* QMs may have the potential to re-alkylate the aged form of AChE and to reverse the side effects of OP toxins (Scheme 1.4).

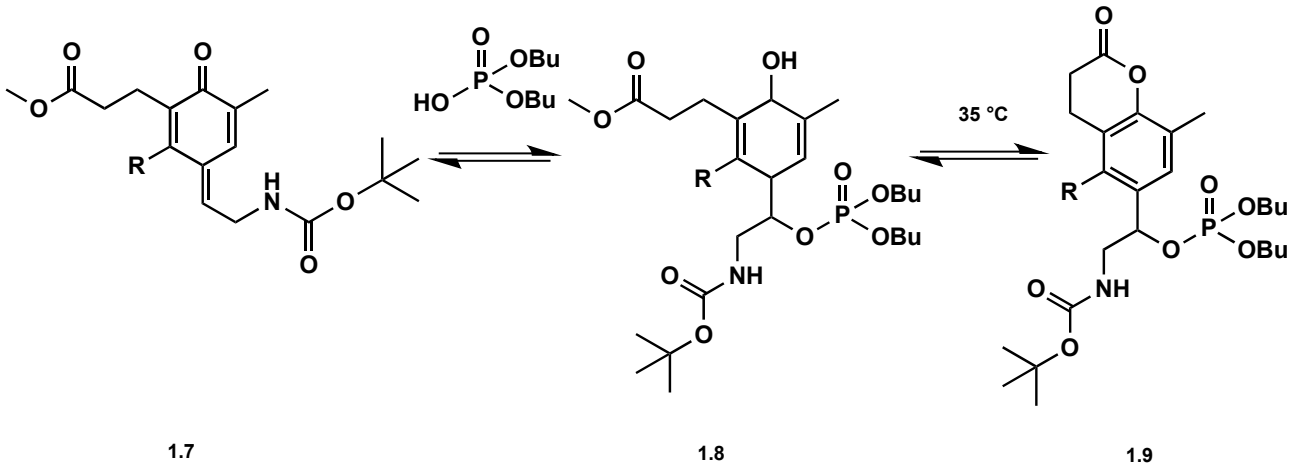

Scheme 1.3. Alkylation of a phosphodiester from a *p*-QM.

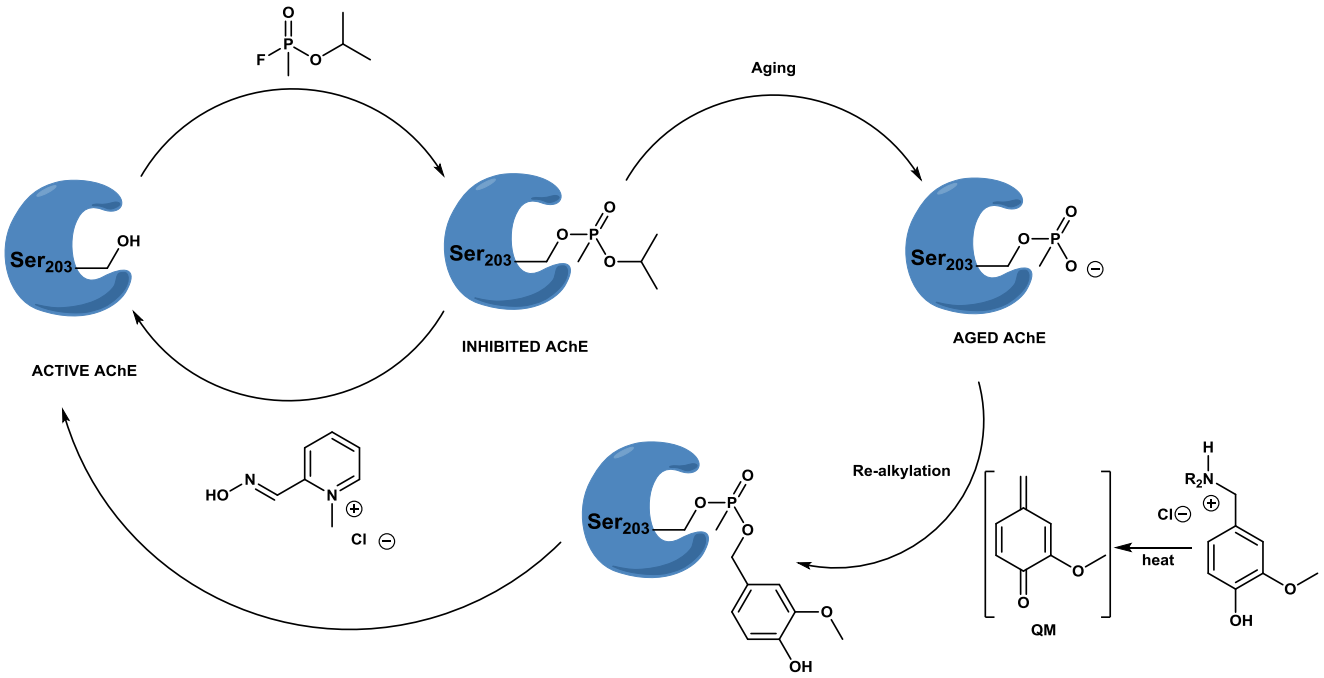

Scheme 1.4. Inhibition and aging from an OP followed by re-alkylation via QMP and oxime**.**

In our current research, there are many possible QMPs that could be envisioned in order to re-alkylate an aged AChE, but it would be an inefficient use of time, money, and resources to synthesize and study an entire library without a high-throughput approach. To narrow the options in order to guide synthetic and experimental efforts, computational methods were used to determine the reactivity and preferred docking pose of each QMP. Computational chemistry has slowly become an enormously

attractive tool for research in recent years because it is efficient in reducing costs and wasted resources. Computational chemistry is also useful in guiding synthetic routes that can determine optimal conditions and design. In general, computation can be defined as using technology to solve complicated mathematical equations for specific theories in quantum mechanics. Computational methods in the field of chemistry can provide ample information including preferred structures, bond strength, stability and chemical properties of molecules as well as the thermodynamics and kinetics of reactions.[7]

Computational methods were used to experimentally test the reactivity of QMs with sulfur-, oxygen-, and nitrogen-centered nucleophiles, H-bonding strength of the alkylated species and substrates, and solvent effects. The use of computational methods aided the synthetic routes of alkylation to more affordable experiments. This was accomplished via Gaussian 09 to perform the following calculations: (1) geometry optimizations of the reactants, intermediates, transition states, and products of the reaction; (2) intrinsic reaction coordinates (IRC) to monitor the entire reaction; and (3) vibrational frequency calculations to classify each stationary point as a minimum or maximum on the potential energy surface by confirming the proper number of imaginary vibrational frequencies. Valetin et al. were successful in developing computational methods to analyze the reactivity of QMs which is the inspiration behind the research being presented.[8]

The goal of using computational methods for this research is twofold: to narrow down a list of 18 QMPs (Figure 1.2) so that the most favorable compounds can be synthesized in the laboratory and with potential to re-alkylate the aged form of AChE. Computational methods were used to analyze the reaction pathways of the pyridine and pyridinium QMPs with a model phosphonate group acting as a nucleophile, and were used to perform docking calculations of each QMP interacting with aged AChE.

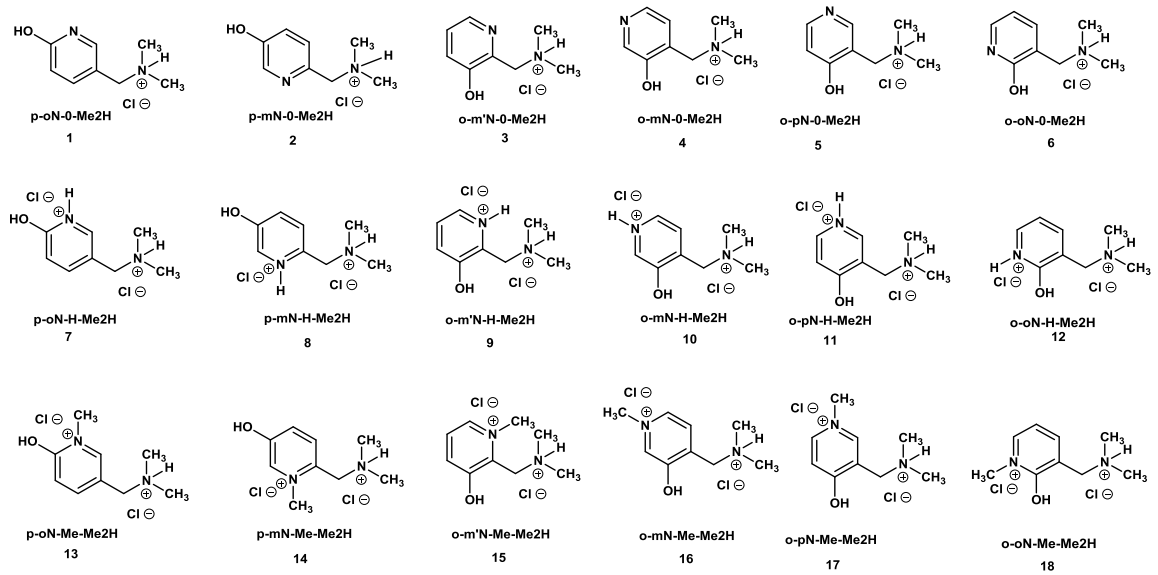

Figure 1.2. The 18 pyridine and pyrimidine QMPs analyzed and studied. 0-Compounds are numbered **1–6**, H-Compounds **7–12**, and Me-Compounds **13–18**.

The naming system used to describe each QMP was created by Dr. Chris Callam. Using p-mN-0-Me2H (**1**) as an example (Figure 2.1): The first letter, "p", describes the position of the benzylic carbon to the hydroxyl group on the ring. "P" is a *para* position and "o" is an *ortho* position. The second and third letters, "o" and "N", tell where the nitrogen is placed inside the ring with respect to the hydroxyl group. The nitrogen can be *para, meta,* or *ortho* to the hydroxyl group. The first number, "0", says that the compound is non-protonated at the nitrogen position within the ring and is a pyridine derivative. The compound can be protonated or methylated making it a pyridinium derivative. The "Me2H" applies to all of the QMPs and shows that the nitrogen bonded to the benzylic carbon also has two methyl groups and one hydrogen atom bonded to it resulting in a positive charge.

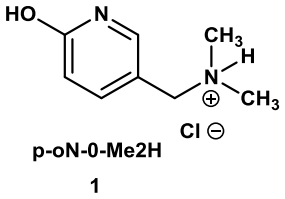

Figure 1.3. p-N-0-Me2H **(1)** QMP describing the naming system.

1.2 References

1. Parenti, Michael. Global Research. "Syria, Sarin, and Casus Belli." Web. (Accessed October 4, 2013).

2. Vijaya Kumar, S.; Fareedullah, M.; Sudhakar Y.; Venkateswarlu, B.; Ashok Kumar, E. *Scholars Research Library*. **2010**, 2 (*4*), 199.

3. Peter, M.G. *Angew*. *Chem. Int. Ed. Engl*. **1989**, *28*, 555.

4. Veldhuyzen, W. F.; Shallop, A. J.; Jones, R. A.; Rokita, S. E. *J. Am. Chem. Soc*. **2001**, *123*, 11126.

5. Modica, E.; Zanaletti, R.; Freccero, M.; Mella, M. *J. Org. Chem*. **2001**, *66*, 41.

6. Bakke, B. A.; McIntosh, M. C.; Turnbull, K. D. *J. Org. Chem*. **2005**, *70*, 4338-4345.

7. Cramer, Christopher J. Essentials of Computational Chemistry. Theories and Models, 2nd ed; Wiley: England, 2004; pp 1-16.

8. Valentin, C. D.; Freccero, M.; Zanaletti, R.; Sarzi-Amadè, M. *J. Am. Chem. Soc*. **2001**, *123*, 8366.

2. Energetics of Mechanisms

2.1 Computational Methods

The computational methods used to determine the energetics of the pyridine and pyrimidine QMPs model the experiment from Valentin et al. Each QMP was built in the GaussView program[1] while the Gaussian09 program[2] was used for all methods and calculations. All steps were calculated at the B3LYP/6-31G* level of theory with water as the solvent for the polarizable continuum model (PCM).[3,4] The following calculations were performed: geometry optimizations; geometry scans for fixed O–C and C–N distances, with and without a model phosphonate depending on the mechanism; transition state scans; vibrational frequency calculations; and intrinsic reaction coordinate searches. Each QMP was created while altering the dihedral of the ring chain to –100º, and –120º making the chain above, below, and parallel with the ring structure. The optimizations were checked for convergence and the energies and dihedral angles were reported. Following the geometry optimizations, the 18 QMPs with the lowest energies (Hartrees) in its specific category (e.g. o-mˈN-0-Me2H and o-mˈN-H-Me2H) were used to perform the mod redundant scans, monitoring the formation of the QM. The constrained geometry scans considered the carbon-amine bond or carbon-oxygen bond from the phosphonate group leaving with 0.1 Å step size at 25 steps for the S_N1 mechanism, and the attacking amine group to displace the phosphonate group from 3.0 Å with a –0.1 Å step size for the S_N2 mechanism. All constrained geometry scans were performed with a phenolate substituent because when the scans were originally calculated with the oxygen as a phenol group, the oxygen would lose the hydrogen to the leaving group. The transition state energies and bond lengths were estimated from the energy peak in the constrained geometry energy diagram or ignored if the scan was asymptotic to a plateau. The estimated transition states were optimized to find the true transition states and were checked for convergence. Frequency calculations were performed on the true transition states to confirm that the transition state contained only one imaginary vibrational frequency along the proper

reaction coordinate.[2,5] If the transition state contained one imaginary frequency, an intrinsic reaction coordinate search was performed to obtain the reactants, transition states, and products of the overall reaction. A final geometry optimization was performed on the reactants and products to confirm the minimum energy conformer was found by the IRC calculation.

2.2 S_N1 Mechanism

As stated in the introduction, there were two ways a QM could potentially re-alkylate the aged AChE: by S_N1 mechanism or S_N2 mechanism. The S_N1 mechanism (Scheme 2.1) involved the amine group leaving (2.1) to form the QM and first transition state (2.2), the intermediates (2.3), the second transition state from the QM-phosphonate group adduct (2.4), and the finalized products (2.5). The non-protonated QMPs were the most energetically favorable for the S_N1 mechanism with the o-oN-0-Me2H QMP (**6**) having the lowest, more stable energy barriers for the *ortho* compounds and the p-oN-0-Me2H QMP (**1**) having the lowest, more stable energy barriers for the *para* compounds.

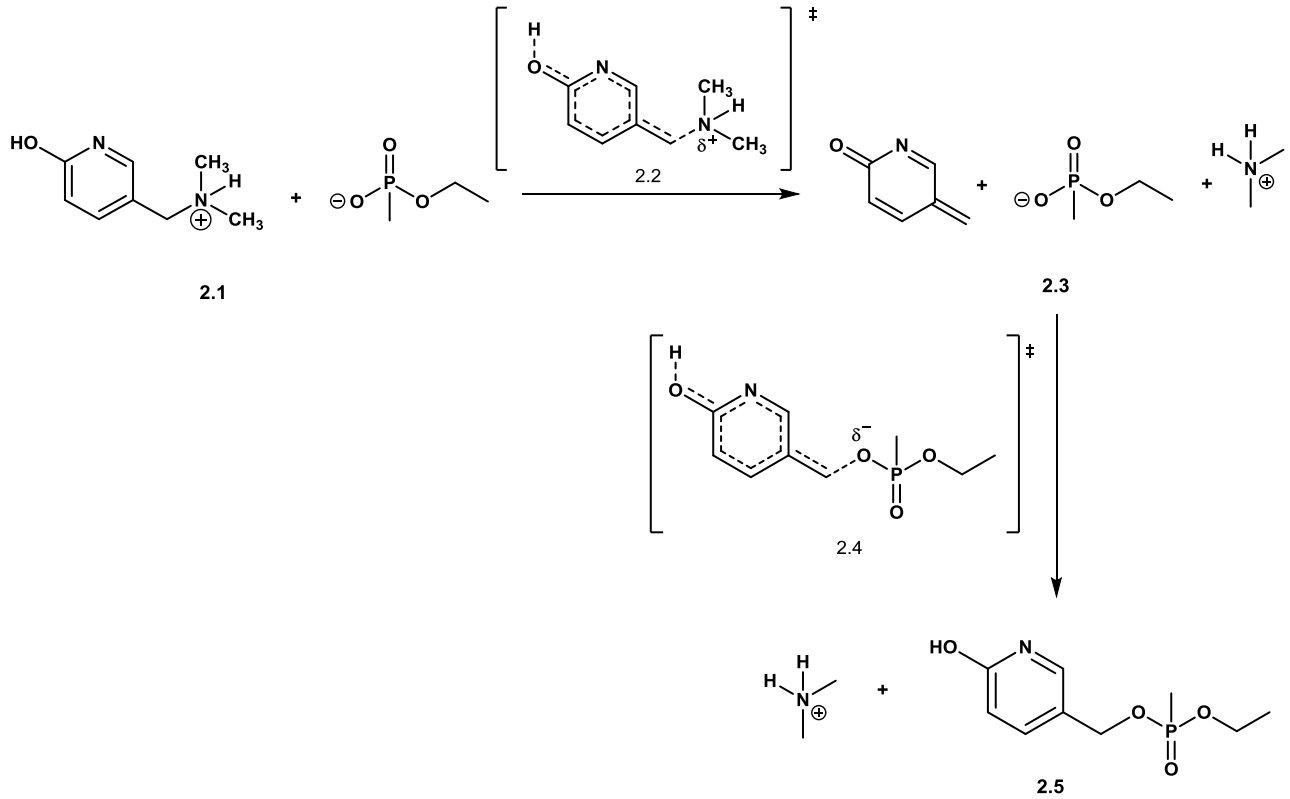

Scheme 2.1. Example of S_N1 mechanism with the p-oN-0-Me2H QMP (**1**).

2.2A: 0-Compounds

The 0-compounds (**1**–**6**) studied were the only compounds that were truly successful in the S_N1 mechanism. The 0-compounds (**1**–**6**) of each QMP were found to have energies of ~ -311750 kcal/mol with the dihedrals ranging from –80° to –160º relative to the ring structure after geometry optimizations (Figure 2.2). The energies and dihedrals reported are the energies where the phenol group is deprotonated because when the protonated oxygen substituent was used in the constrained geometry scans, the hydrogen was taken from the leaving amine or phosphonate group (Table 2.1).

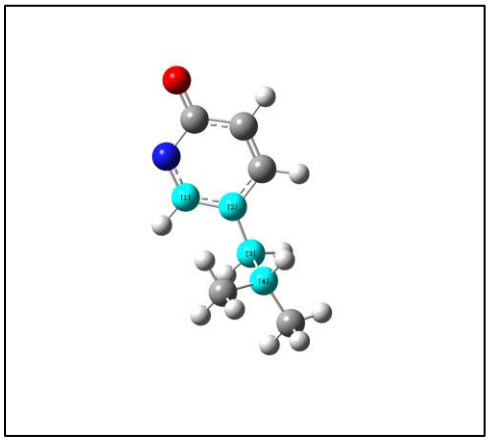

Figure 2.1. Highlighted atoms represent the dihedral angle –99.1° measured for the QMP p-oN-0-Me2H (**1**).

Name	Rel. Deprotonated Energy (kcal/mol)	Dihedral Angle
p-oN-0-Me2H (**1**)	6.275	–99.1
o-oN-0-Me2H (**6**)	0	–137.1

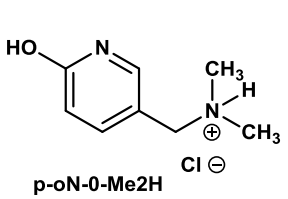

p-oN-0-Me2H

1

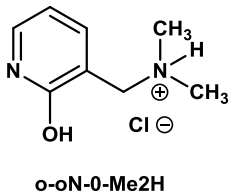

o-oN-0-Me2H

6

Table 2.1. The two most energetically favorable QMPs for the S_N1 mechanism after geometry optimizations. (**1**) is calculated relative to (**6**).

The first constrained geometry scans for the S_N1 mechanism were calculated for the formation of the QM from the amine group leaving. The transition states were estimated from the highest energy geometry from the scan output, which showed the bond distance between the benzylic carbon and nitrogen to be an average of 2.5 Å. Only the 0-compounds (o-pN-0-Me2H (**5**) being an exception) were found to have such a peak while the remaining H- and Me-compounds were found to be asymptotic (Figure 2.3).

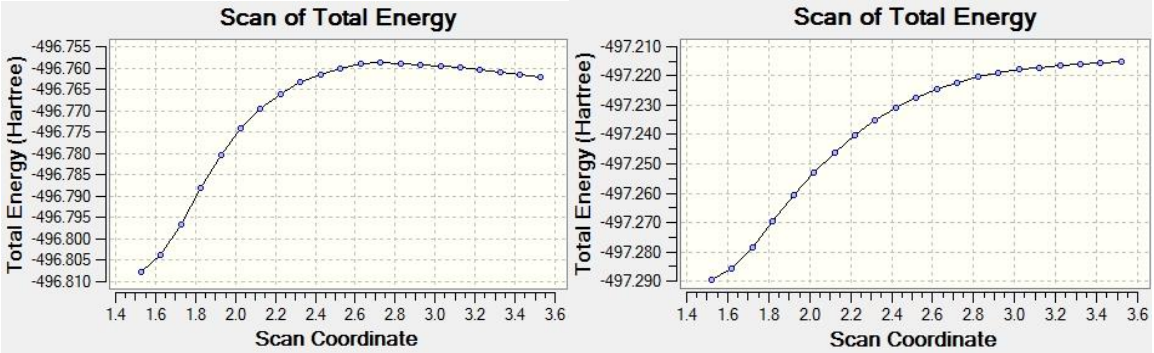

Figure 2.2. Difference between peak energies and asymptotic scans. o-oN-0-Me2H (**6**, left) o-oN-H-Me2H (**12**, right).

The second constrained geometry scan calculated the second transition state by having the phosphonate group leave. This mimicked the potential re-alkylation of the phosphonate group from the QM. Again, only the 0-compounds had peak energies with an average bond length of 2.13 Å between the benzylic carbon and oxygen anion. Transition state calculations were performed on the estimated transition state geometry from each step of the reaction in attempt to find the true transition state. The C-N bond length was ~2.6 Å (Figure 2.4A) while the C-O was shorter at ~2.1 Å (Figure 2.4B). To ensure that these transition states were valid, only one imaginary frequency along the proper reaction coordinate should have been visible.[4]

(a) 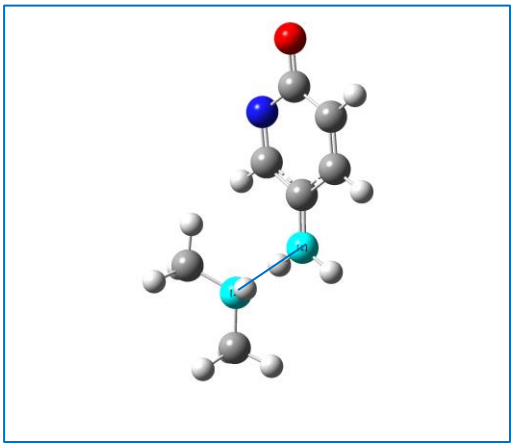 (b) 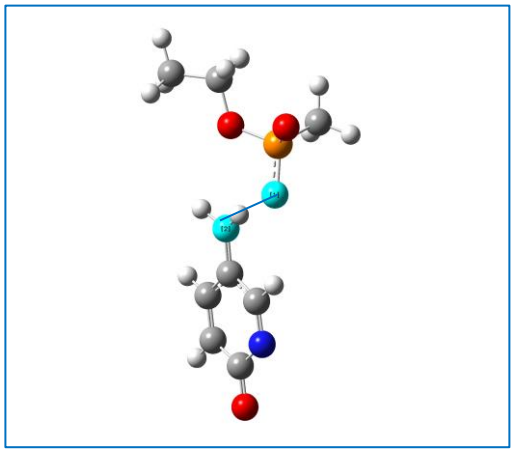

Figure 2.3. QMP p-oN-0-Me2H **(1)**. (a) Transition state C-N bond = 2.53 Å. (b) Transition state C-O bond = 2.13 Å.

After performing the above calculations, the total reaction coordinate for each compound was plotted. The energies for each step were calculated relative to the reactants (kcal/mol). Ideally, the optimizations of the reactants and products from the IRC scans would serve as the desired energies, but because the protonated and methylated compounds did not contain an energy peak in their constrained geometry scans, the total reaction coordinate was calculated in a slightly different way than the S_N2 mechanism. The asymptotic scans did not have a true transition state because the scans did not converge and the bond lengths were too far, typically ~4.37 Å, after performing a "no eigentest" transition state search. Instead of taking the energy from the transition state calculation, the last point on the asymptotic scans of the formation of the QM and alkylation of the phosphonate group were optimized to obtain the energy of the "transition states". The 0-compounds were the only compounds that used the actual transition state energies, and the rest of the reaction coordinate was calculated with the same method as the H- and Me- compounds to have consistency. The total reactant energy was calculated from the optimized QMP and adding the optimized phosphonate group, the intermediates were calculated by optimizing the QM by itself and adding the energies of the optimized amine and

phosphonate group, and the total product energy was calculated from the alkylated phosphonate group and adding the optimized amine (Table 2.2 and Figure 2.5).

Name	Reactant Energy (kcal/mol)	TS1 Energy (kcal/mol)	C–N Bond Length (Å)	Intermediate Energy (kcal/mol)	TS2 Energy (kcal/mol)	C–O Bond Length (Å)	Product Energy (kcal/mol)
(**6**)	0	30.64	2.76	30.51	30.01	2.14	18.37
(**1**)	0	22.00	2.85	21.84	23.61	2.09	13.17

Table 2.2. Total reaction coordinate calculations of o-oN-0-Me2H (**6**) and p-oN-0-Me2H (**1**) for the S_N1 mechanism.

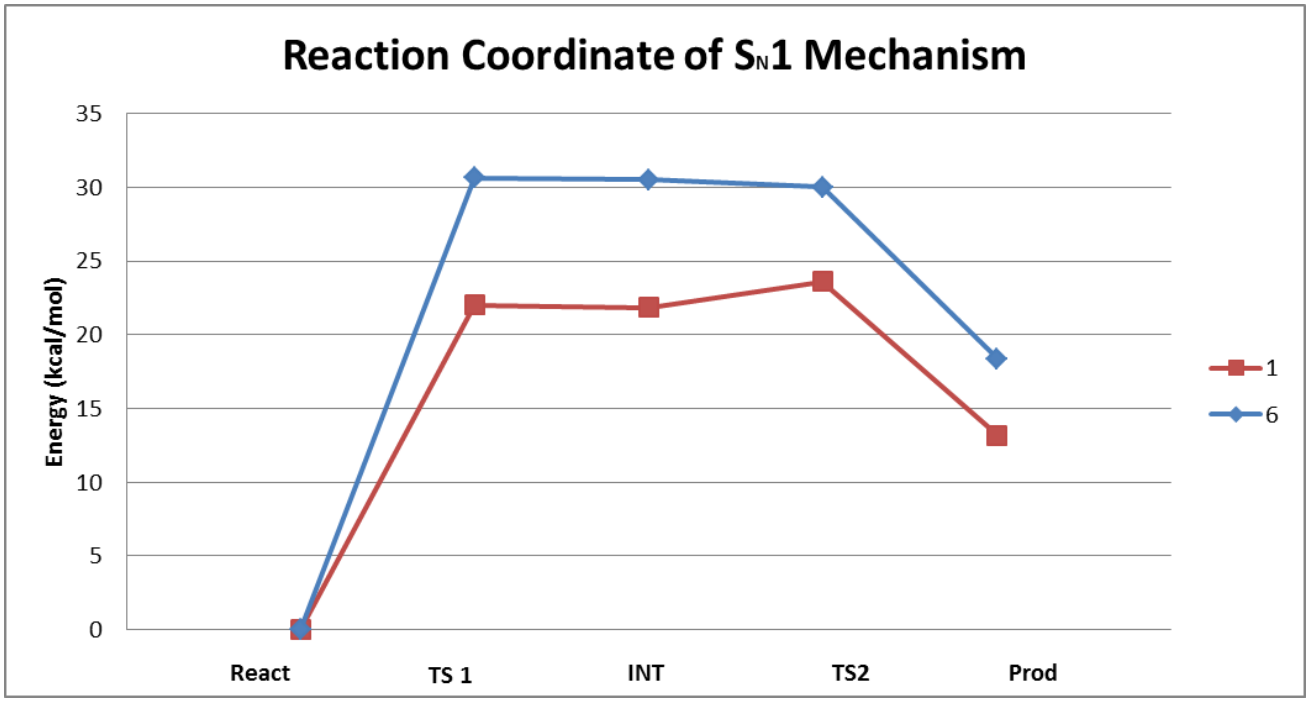

Figure 2.4. Reaction coordinate diagram of o-oN-0-Me2H (**6**) and p-oN-0-Me2H (**1**) for the S_N1 mechanism.

The reaction coordinate diagram shows that the p-oN-0-Me2H QMP (**1**) is significantly more energetically stable than the o-oN-0Me2H QMP (**6**). The p-oN-0-Me2H QMP (**1**) has lower energy barriers for the first and second transition states by 8.64 and 6.4 kcal/mol, respectively. For the overall reaction, p-oN-0-Me2H (**1**) is also more stable by 5.2 kcal/mol. It is difficult to tell what the rate

determining step is in the reaction because the p-oN-0-Me2H QMP (**1**) has a larger second energy barrier while the o-oN-0-Me2H QMP (**6**) has a larger first energy barrier. The estimated asymptotic energies would agree that the first energy barrier is the largest and the amine leaving is the rate determining step; however, the remaining unprotonated *ortho* and *para* QMPs show that the alkylation of the phosphonate group is rate determining (Appendix A and B). Because the 0-compounds (**1**–**6**) were the only successful compounds for the S_N1 mechanism, it can be concluded that the non-protonated compounds react via an S_N1 mechanism.

2.3 S_N2 Mechanism

The re-alkylation of the aged AChE could potentially occur by an S_N2 mechanism (Scheme 2.2). Originally the S_N2 mechanism involved the phosphonate group (2.6) attacking the benzylic carbon of the QMP (2.7) and displacing the amine (2.9), but there was too much interference with the incoming nucleophile which caused the calculations to end with an error after 5 steps. The mechanism was then analyzed with the amine displacing the bound phosphonate group which provided a successful mod redundant scan and the proper transition state (2.8). The methylated QMPs were determined to be the most energetically favorable for the S_N2 mechanism with the o-oN-Me-Me2H (**18**) compound being lowest for the *ortho* compounds and p-mN-Me-Me2H (**14**) being lowest for the *para* compounds.

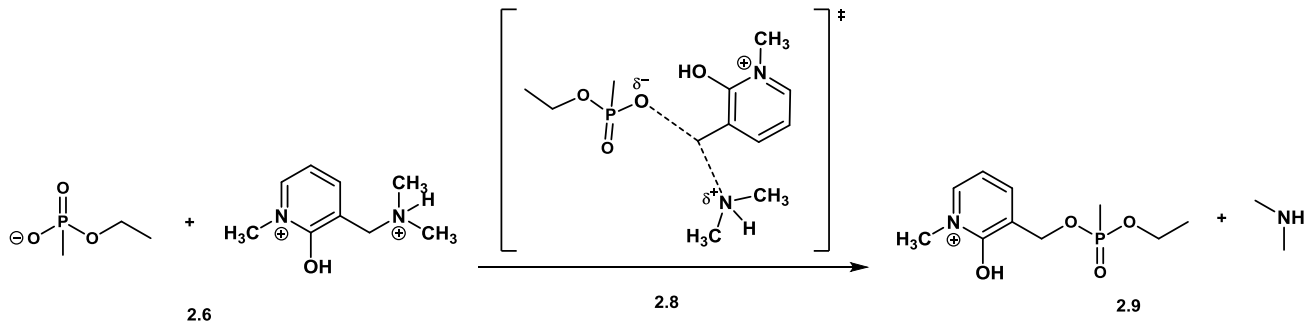

Scheme 2.2. Example of the S_N2 mechanism with the o-oN-Me-Me2H QMP (18).

2.3A: Me-Compounds

Unlike the S_N1 mechanism, the Me-compounds for the S_N2 mechanism were a success and were the most energetically favorable. The process for calculating the S_N2 mechanism was the same as the S_N1 mechanism, yet slightly different because there was only one transition state to calculate and no intermediates. The constrained geometry scans contained a max peak for each methylated QMP which allowed for proper determination of the true transition state. While calculating the transition states, a "no eigentest" transition state search was performed so that the calculations could optimize completely and converge. The transition state for the S_N2 mechanism had a C–O bond length between 1.96 and 2.05 Å while the C–N bond was between 2.26 and 2.41 Å (Figure 2.6).

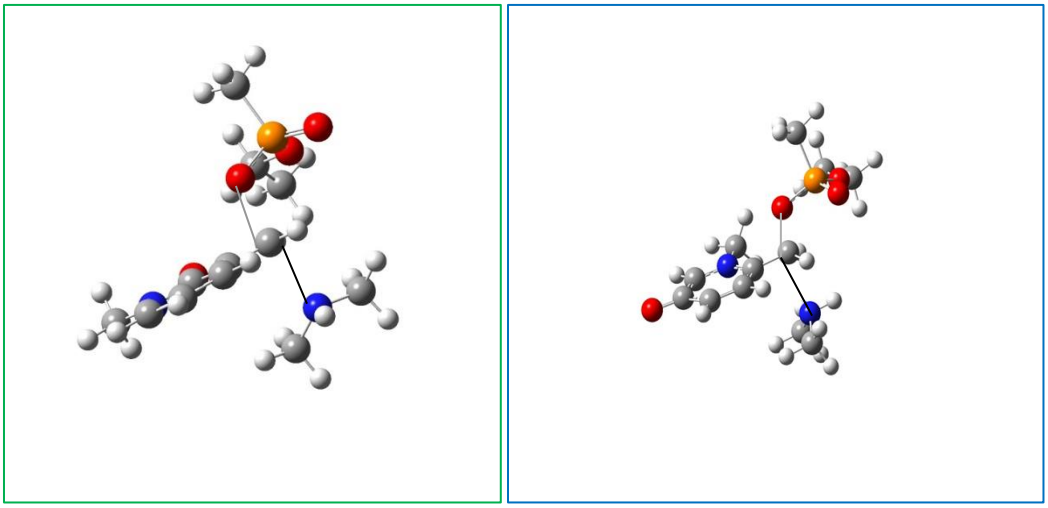

Figure 2.5. Left: QMP o-oN-Me-Me2H (**18**) transition state: C–N = 2.21Å and C–O = 1.94 Å. Right: QMP p-mN-Me-Me2H (**14**) transition state: C–N = 2.04 Å and C–O = 2.05 Å.

Vibrational frequency calculations were performed ensuring that the transition state had only one imaginary frequency along the proper reaction coordinate which was typically ~ 460 *i* cm^{-1}.[4] Geometry optimizations from the IRC scans provided the final energies of the reactants, transition states, and products. The total reaction coordinates were calculated relative to the reactants in kcal/mol (Table 2.3 and Figure 2.7). The two most energetically favorable QMPs were the o-oN-Me-Me2H (**18**) and the p-mN-Me-Me2H (**14**) compounds. The reaction barriers differed by 3.06 kcal/mol with the p-mN-Me-Me2H QMP (**14**) having the lower barrier and more stable product formation.

Name	Reactant Energy (kcal/mol)	TS Energy (kcal/mol)	C–N Bond Length (Å)	C–O Bond Length (Å)	Product Energy (kcal/mol)
o-oN-Me-Me2H (**18**)	0	33.33	2.28	1.98	12.54
p-mN-Me-Me2H (**14**)	0	30.27	2.41	2.05	10.65

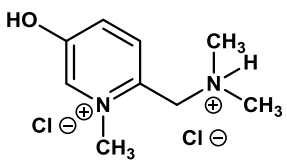

p-mN-Me-Me2H

14

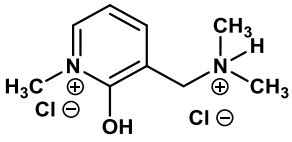

o-oN-Me-Me2H

18

Table 2.3. Total reaction coordinate calculations of o-oN-Me-Me2H (**18**) and p-mN-Me-Me2H (**14**) for the S_N2 mechanism.

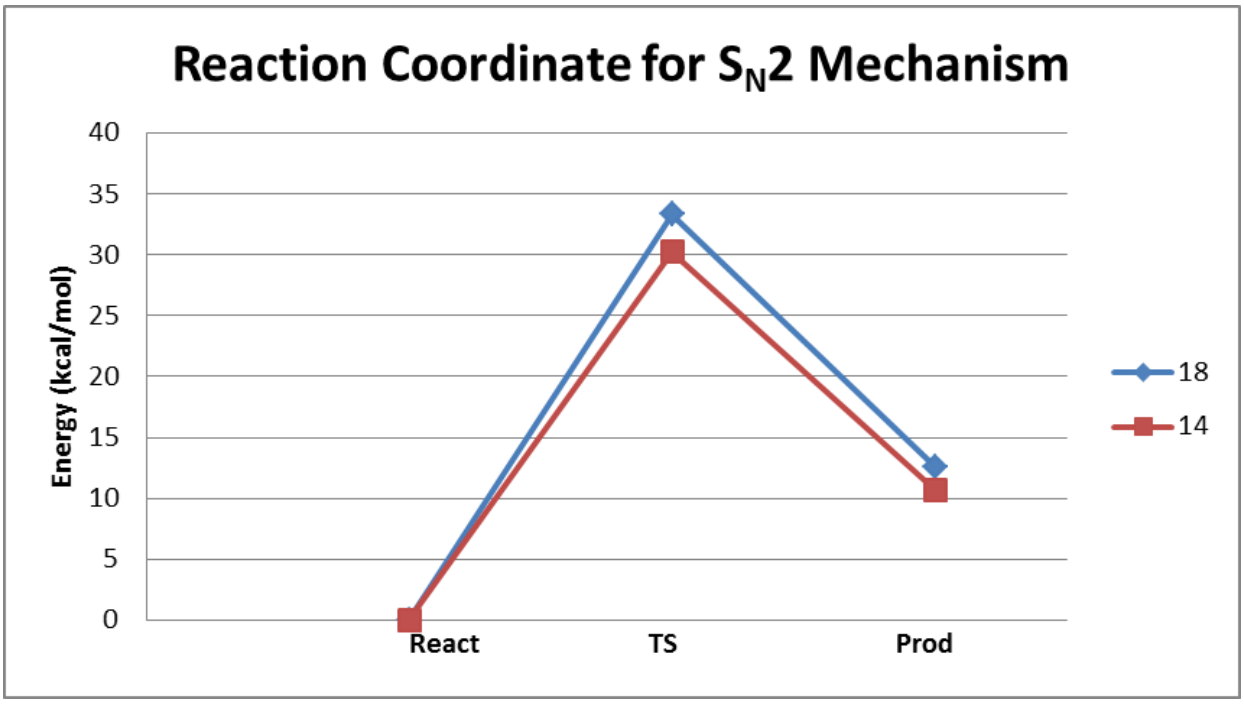

Figure 2.6. Reaction coordinate diagram of o-oN-Me-Me2H (**18**) and p-mN-Me-Me2H (**14**) for the S_N2 mechanism.

2.4 References

1. GaussView, Version 5, Dennington, Roy; Keith, Todd; Millam, John. Semichem Inc., Shawnee Mission, KS, 2009.

2. Gaussian 09, Revision D.01, Frisch, M. J.; Trucks, G. W.; Schlegel, H. B.; Scuseria, G. E.; Robb, M. A.; Cheeseman, J. R.; Scalmani, G.; Barone, V.; Mennucci, B.; Petersson, G. A.; Nakatsuji, H.; Caricato, M.; Li, X.; Hratchian, H. P.; Izmaylov, A. F.; Bloino, J.; Zheng, G.; Sonnenberg, J. L.; Hada, M.; Ehara, M.; Toyota, K.; Fukuda, R.; Hasegawa, J.; Ishida, M.; Nakajima, T.; Honda, Y.; Kitao, O.; Nakai, H.; Vreven, T.; Montgomery, J. A., Jr.; Peralta, J. E.; Ogliaro, F.; Bearpark, M.; Heyd, J. J.; Brothers, E.; Kudin, K. N.; Staroverov, V. N.; Kobayashi, R.; Normand, J.; Raghavachari, K.; Rendell, A.; Burant, J. C.; Iyengar, S. S.; Tomasi, J.; Cossi, M.; Rega, N.; Millam, N. J.; Klene, M.; Knox, J. E.; Cross, J. B.; Bakken, V.; Adamo, C.; Jaramillo, J.; Gomperts, R.; Stratmann, R. E.; Yazyev, O.; Austin, A. J.; Cammi, R.; Pomelli, C.; Ochterski, J. W.; Martin, R. L.; Morokuma, K.; Zakrzewski, V. G.; Voth, G. A.; Salvador, P.; Dannenberg, J. J.; Dapprich, S.; Daniels, A. D.; Farkas, Ö.; Foresman, J. B.; Ortiz, J. V.; Cioslowski, J.; Fox, D. J. Gaussian, Inc., Wallingford CT, 2009.

3. Frisch, M. J.; Pople, J. A.; Binkley, J. S. *J. Chem. Phys*. **1984**, *80*, 3265.

4. Lee, C.; Yang, W.; Parr, R. G. *Phys Rev B* **1988**, *37*, 785.

5. http://www.chemcraftprog.com

3. Docking Calculations

3.1 Docking Protocol

The molecular docking simulations involved taking each optimized QMP and locating the optimal orientations for these ligands inside the active site of an aged form of the human AChE enzyme. For these simulations, the ligand was flexible, but the aged AChE structure was kept rigid. Merz-Kollman charge calculations were performed on the optimized QMPs using the Gaussian09 prorgram[1] at the B3LYP/6-311+G** level of theory to prepare the QMPs for docking.[2,3] Thirteen different snapshots of an aged human AChE were created from Jeremy Beck's molecular dynamic (MD) simulations.[4] In the original Protein Data Bank structure for the human AChE, Fasciculin is bound in the active site. Thus, Fasciculin was removed from the structure, and an aged OP compound was built within the active site by overlaying the AChE with a crystal structure of an aged non-human AChE. A model QMP was then docked into this AChE structure and MD simulations were ran. Snapshots were taken of the MD runs and were used for the docking calculations of the pyridine and pyridinium QMPs. The snapshots contained a box simulating the 20 Å gorge with the primary and secondary binding sites where the QMPs were docked. All molecular docking simulations were performed using AutoDock.[5] All 18 QMPs were analyzed for each frame and the binding energies and population of the top three clusters were recorded. A point system was created to identify the best docked molecules. Each ligand needed to have the benzylic carbon within 3.7 Å of the reactive oxygen on the serine residue of the AChE in order for the QMP to be in a productive binding mode.. The molecule would then receive 3 points if it was the most populated cluster with a good pose, 2 points for the second most populated and a good pose, 1 point for the least populated with a good pose, and 0.5 points for any other poses in a good position allowing a molecule to receive a maximum of 6.5 points. A "good pose" was defined as the QMP being deep inside the gorge and the benzylic carbon of the

QMP facing the reactive oxygen on Ser with the leaving amine group facing down and away to prevent any interfering interactions (Figure 3.1).

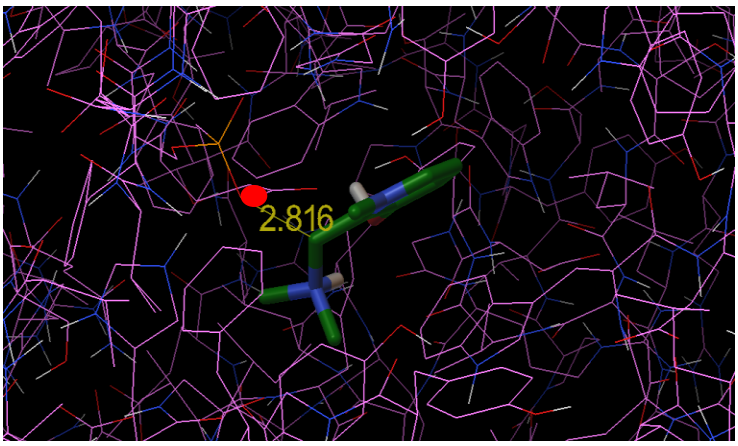

Figure 3.1. Docking calculation showing a good pose with the amine group facing down and away, benzylic carbon facing reactive oxygen on Ser (red dot). QMP: o-mˈN-Me-Me2H (**15**), binding energy = -4.8, frame 1000.

3.2 Docking Calculations

Using the point system described in the protocol section, it was determined that the methylated compounds, specifically o-mN-Me-Me2H (**16**) and o-mˈN-Me-Me2H (**15**), were the QMPs that docked the best inside the aged AChE (Table 3.1), meaning they contained the most number of poses where the amine group was facing down and away from the reactive oxygen on Ser while the benzylic carbon was free to react with the oxygen. The docking calculations showed that there were two more preferential poses of the QMPs that have potential to re-alkylate the aged AChE. The second preferential pose (Figure 3.2) has the QMP rotated 180˚ from the first preferential pose where the amine is facing up and away, yet the benzylic carbon is still free to react with the oxygen. The last preferential pose has the QMP rotated 90˚ from the primary preferential pose (Figure 3.3). This pose could potentially work because the amine is facing away from the reactive oxygen, but the phenol group on the ring could interfere with the benzylic carbon.

Name	Points
o-mN-0-Me2H (**4**)	6.5
o-oN-0-Me2H (**6**)	15.0
o-pN-0-Me2H (**5**)	11.0
o-mN-H-Me2H (**10**)	9.0
o-oN-H-Me2H (**12**)	12.0
o-pN-H-Me2H (**11**)	11.5
o-mN-Me-Me2H (**16**)	29.5
o-oN-Me-Me2H (**18**)	24.5
o-pN-Me-Me2H (**17**)	16.0
p-mN-0-Me2H (**2**)	11.0
p-oN-0-Me2H (**1**)	13.0
o-m'N-0-Me2H (**3**)	18.0
p-mN-H-Me2H (**8**)	13.0
p-oN-H-Me2H (**7**)	21.0
o-m'N-H-Me2H (**9**)	25.0
p-mN-Me-Me2H (**14**)	19.0
p-oN-Me-Me2H (**13**)	24.0
o-m'N-Me-Me2H (**15**)	43.0

Table 3.1. List of each QMP and its respective point total for the docking calculations. See text for the scoring algorithm for each docked orientation in aged AChE.

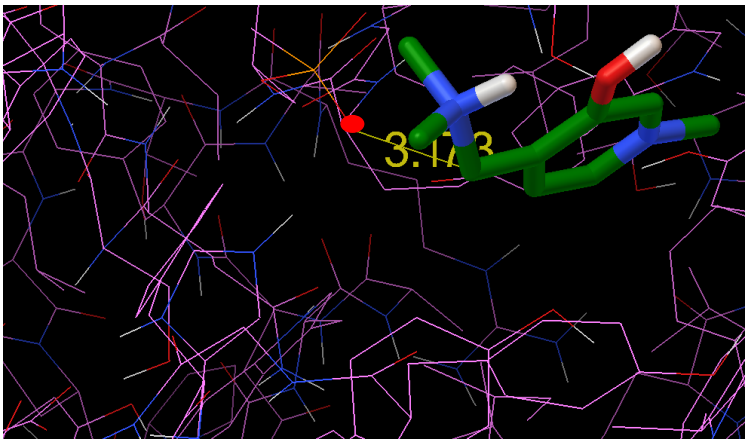

Figure 3.2. QMP: o-mN-Me-Me2H (**16**), binding energy = –4.11, frame 0400. Second preferential pose with amine facing up and away with benzylic carbon facing reactive oxygen on Ser (red dot).

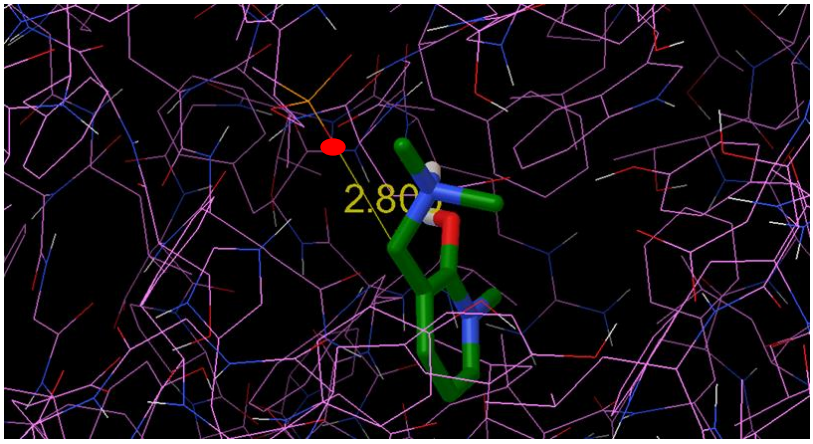

Figure 3.3. QMP: o-oN-Me-Me2H (**18**), binding energy = -4.67, frame 0400. Third preferential pose with amine facing away but phenol possibly interfering.

Docking calculations were also performed on a normal AChE enzyme to examine the potential reactivity of the QMP and the active site. The majority of the poses had the QMPs on the outside of the gorge ~3.7 Å or greater from the active site which is desired because it is important that the QMPs do not inhibit the enzyme.

The docking calculations indicated that it was not the energetics of the mechanisms that determined how well the QMPs docked, but it was the shape of the QMP that governed the docking. The *ortho-meta* QMPs docked the best yet were not the most favorable energetically for either mechanism.

3.3 References

1. Gaussian 09, Revision D.01, Frisch, M. J.; Trucks, G. W.; Schlegel, H. B.; Scuseria, G. E.; Robb, M. A.; Cheeseman, J. R.; Scalmani, G.; Barone, V.; Mennucci, B.; Petersson, G. A.; Nakatsuji, H.; Caricato, M.; Li, X.; Hratchian, H. P.; Izmaylov, A. F.; Bloino, J.; Zheng, G.; Sonnenberg, J. L.; Hada, M.; Ehara, M.; Toyota, K.; Fukuda, R.; Hasegawa, J.; Ishida, M.; Nakajima, T.; Honda, Y.; Kitao, O.; Nakai, H.; Vreven, T.; Montgomery, J. A., Jr.; Peralta, J. E.; Ogliaro, F.; Bearpark, M.; Heyd, J. J.; Brothers, E.; Kudin, K. N.; Staroverov, V. N.; Kobayashi, R.; Normand, J.; Raghavachari, K.; Rendell, A.; Burant, J. C.; Iyengar, S. S.; Tomasi, J.; Cossi, M.; Rega, N.; Millam, N. J.; Klene, M.; Knox, J. E.; Cross, J. B.; Bakken, V.; Adamo, C.; Jaramillo, J.; Gomperts, R.; Stratmann, R. E.; Yazyev, O.; Austin, A. J.; Cammi, R.; Pomelli, C.; Ochterski, J. W.; Martin, R. L.; Morokuma, K.; Zakrzewski, V. G.; Voth, G. A.; Salvador, P.; Dannenberg, J. J.; Dapprich, S.; Daniels, A. D.; Farkas, Ö.; Foresman, J. B.; Ortiz, J. V.; Cioslowski, J.; Fox, D. J. Gaussian, Inc., Wallingford CT, 2009.

2. Breneman, C. M.; Wiberg, K. B. *J. Comput. Chem*. **1990**, *11*, 361.

3. Singh, U. C.; Kollman, P. A. *J. Comput. Chem.* **1984**, *5*, 129.

4. Beck, J. M., Ph.D. thesis, The Ohio State University, 2011

5. Morris, G. M., Huey, R., Lindstrom, W., Sanner, M. F., Belew, R. K., Goodsell, D. S. and Olson, A. J. (2009) Autodock4 and AutoDockTools4: automated docking with selective receptor flexiblity. J. Computational Chemistry 2009, 16: 2785-91.

4. Conclusions and Current Work

4.1 Conclusions

For both the S_N1 and S_N2 mechanism, the two families that contained the most energetically favorable QMPs were the p-mN and the o-oN families. The 0-compounds (**1**–**6**) within these families formed the QM and would re-alkylate the phosphonate group most likely via an S_N1 reaction while the Me-compounds (**13**–**18**) would re-alkylate the phosphonate group via an S_N2 reaction. Despite the p-mN and o-oN QMPs are the most favorable when performing the substitution, they were not the best structures for docking inside the aged AChE. The docking calculations showed that it was not necessarily the lowest energy QMPs that docked the best, but more dependent on the shape of the QMP. The best docking ligands were the o-mN-Me-2H (**16**) and o-mˈN-Me2H (**15**) QMPs (Table 4.1). The primary pose of the best docked QMPs had the amine group facing down and away in the gorge while the benzylic carbon was directly facing the reactive oxygen on the Ser.

Name	TS Energy (kcal/mol)	Points
o-oN-Me-Me2H (**18**)	29.6	24.5
o-mN-Me-Me2H (**16**)	34.38	29.5
p-mN-Me-Me2H (**14**)	30.27	19
o-mˈN-Me-Me2H (**15**)	34.91	43

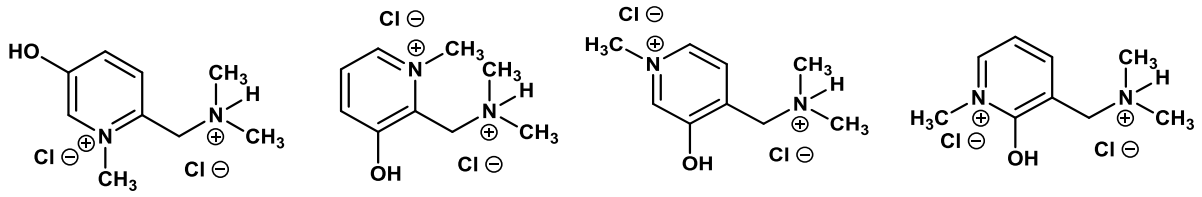

Table 4.1. The top 4 QMPs based on docking reactivity and the four that will be used for molecular dynamic simulations.

4.2 Current Work

The molecular docking simulations did use a number of different snapshots of a molecular dynamics trajectory; however, the actual molecular docking simulations were performed with a flexible ligand (QMP), but a rigid protein (aged AChE). To investigate the role of structural relaxation on the AChE-QMP interaction, I am currently exploring molecular dynamics simulations for specific AChE-QMP complexes. Specifically, molecular dynamic simulations are being performed on two of the top 4 QMPs: the o-mˈN-Me-Me2H (**15**) and p-mN-Me-Me2H (**14**). These molecular dynamic simulations will analyze more accurately the reactivity between the ligand and the active site of an aged AChE with hope of becoming closer to discovering compounds that can re-alkylate an aged AChE to prevent diseases, nerve damage, and even death from OP exposure.

Appendix A

Energy, mod redundant scans, TS tables

Geometry Optimizations of 18 QMPs

Name	Rel. Protonated Energies (kcal/mol)	Rel. Deprotonated Energies (kcal/mol)	Dihedral
o-mN-0-Me2H (**4**)[1]	5.65	6.90	-123.63
o-oN-0-Me2H (**6**)[1]	2.51	0.00	-100.97
o-pN-0-Me2H (**5**)[1]	5.02	1.88	-101.24
o-m'N-0-Me2H (**3**)[2]	4.39	10.67	-162.74
p-oN-0-Me2H (**1**)[2]	0.00	6.27	-100.43
p-mN-0-Me2H (**2**)[2]	5.65	13.18	-81.05
*Dihedrals are reported for the protonated O optimizations			

Table A1: Geometry optimizations of the 0-QMPs. Relative energies are calculated with respect to the lower energy QMP.

	Rel. Protonated Energies (kcal/mol)	Rel. Deprotonated Energies (kcal/mol)	Dihedral
o-mN-H-Me2H (**10**)[1]	6.90	13.80	-101.71
o-oN-H-Me2H (**12**)[1]	2.51	0.00	-99.26
o-pN-H-Me2H (**11**)[1]	0.63	4.39	-100.73
o-m'N-H-Me2H (**9**)[2]	5.81	18.82	-97.48
p-oN-H-Me2H (**7**)[2]	0.00	3.14	-107.17
p-mN-H-Me2H (**8**)[2]	5.67	20.71	-69.61
*Dihedrals are reported for the protonated O optimizations			

Table A2: Geometry optimizations of the H-QMPs. Relative energies are calculated with respect to the lower energy.

	Rel. Protonated Energies (kcal/mol)	Rel. Deprotonated Energies (kcal/mol)	Dihedral
o-mN-Me-Me2H (**16**)[1]	6.27	11.30	-102.44
o-oN-Me-Me2H (**18**)[1]	1.88	0.00	80.62
o-pN-Me-Me2H (**17**)[1]	0.63	1.88	-99.89
o-m'N-Me-Me2H (**15**)[2]	7.53	20.71	-89.92
p-oN-Me-Me2H (**13**)[2]	0.00	0.63	-109.62
o-m'N-Me-Me2H (**14**)[2]	8.16	18.83	-94.31
*Dihedrals are reported for the protonated O optimizations			

Table A3: Geometry optimizations of the Me-QMPs. Relative energies are calculated with respect to the lower energy.

S_N1 Mod Redundant Scans of 18 QMPs. "-" Indicates no true transition state found.

Name	Rel. Peak 1 Energy (kcal/mol)	C-N Length (Å)	Rel. Peak 2 Energy (kcal/mol)	C-O Length (Å)
o-mN-0-Me2H (**4**)[1]	11.92	2.62	10.67	2.13
o-oN-0-Me2H (**6**)[1]	2.51	2.72	0.63	2.13
o-pN-0-Me2H(**5**)[1]	-	-	3.14	2.23
p-mN-0-Me2H (**2**)[2]	6.90	2.52	6.90	2.13
p-oN-0-Me2H (**1**)[2]	0.00	2.53	0.00	2.13
o-m'N-0-Me2H (**3**)[2]	8.16	2.60	7.53	2.03

Table A4. Mod redundant S_N1 scans of the 0-QMPs. Relative energies are calculated with respect to the lower peak.

S_N2 Mod Redundant Scans of 18 QMPs

Name	Rel. Peak 1 Energy (kcal/mol)	C-N Length (Å)	C-O Length (Å)
o-mN-0-Me2H (**4**)[1]	6.90	2.30	1.61
o-oN-0-Me2H (**6**)[1]	1.25	2.30	1.66
o-pN-0-Me2H (**5**)[1]	2.51	2.30	1.64
p-mN-0-Me2H (**2**)[2]	8.78	2.30	1.65
p-oN-0-Me2H (**1**)[2]	0.00	2.40	1.60
o-m'N-0-Me2H (**3**)[2]	5.65	2.30	1.61

Table A5. Mod redundant S_N2 scans of the 0-QMPs. Relative energies are calculated with respect to the lower energy peak.

Name	Rel. Peak 1 Energy (kcal/mol)	C-N Length (Å)	C-O Length (Å)
o-mN-H-Me2H (**10**)[1]	19.45	2.30	2.80
o-oN-H-Me2H (**12**)[1]	0.00	2.30	1.58
o-pN-H-Me2H (**11**)[1]	5.65	2.30	1.59
p-mN-H-Me2H (**8**)[2]	21.34	2.20	1.68
p-oN-H-Me2H (**7**)[2]	1.88	2.30	1.60
o-m'N-H-Me2H (**9**)[2]	16.32	2.30	1.57

Table A6: Mod redundant S_N2 scans of the H-QMPs. Relative energies are calculated with respect to the lower energy peak.

Name	Rel. Peak 1 Energy (kcal/mol)	C-N Length (Å)	C-O Length (Å)
o-mN-Me-Me2H (**16**)[1]	15.69	2.30	1.58
o-oN-Me-Me2H (**18**)[1]	0.00	2.30	1.59
o-pN-Me-Me2H (**17**)[1]	6.90	2.30	1.59
p-mN-Me-Me2H (**14**)[2]	20.08	2.30	1.57
p-oN-Me-Me2H (**13**)[2]	2.51	2.40	1.54
o-m'N-Me-Me2H (**15**)[2]	16.32	2.30	1.57

Table A7: Mod redundant S_N2 scans of the Me-QMPs. Relative energies are calculated with respect to the lower energy peak.

Appendix B

Reaction coordinate tables and diagrams

S_N1 Data

Name	Reactant Energy (kcal/mol)	TS1 Energy (kcal/mol)	C-N Bond Length (Å)	Intermediate Energy (kcal/mol)	TS2 Energy (kcal/mol)	C-O Bond Length (Å)	Product Energy (kcal/mol)
o-mN-0-Me2H (**4**)	0.00	33.66	2.78	33.62	33.91	2.16	17.40
o-oN-0-Me2H (**6**)	0.00	30.64	2.76	30.51	30.01	2.14	18.37
o-pN-0-Me2H (**5**)	0.00	32.60	-	33.24	31.92	2.18	17.92
o-mN-H-Me2H (**10**)	0.00	47.61	-	48.54	44.43	-	14.92
o-oN-H-Me2H (**12**)	0.00	46.39	-	47.05	43.13	-	13.10
o-pN-H-Me2H (**11**)	0.00	48.48	-	49.75	46.57	-	13.82
o-mN-Me-Me2H (**16**)	0.00	45.74	-	46.07	42.00	-	14.88
o-oN-Me-Me2H (**18**)	0.00	42.19	-	43.04	38.61	-	10.55
o-pN-Me-Me2H (**17**)	0.00	46.45	-	47.47	43.52	-	13.87

Table B1: Reaction coordinate energies for the S_N1 data of the *ortho* QMPs. Energies are calculated relative to reactants.[1]

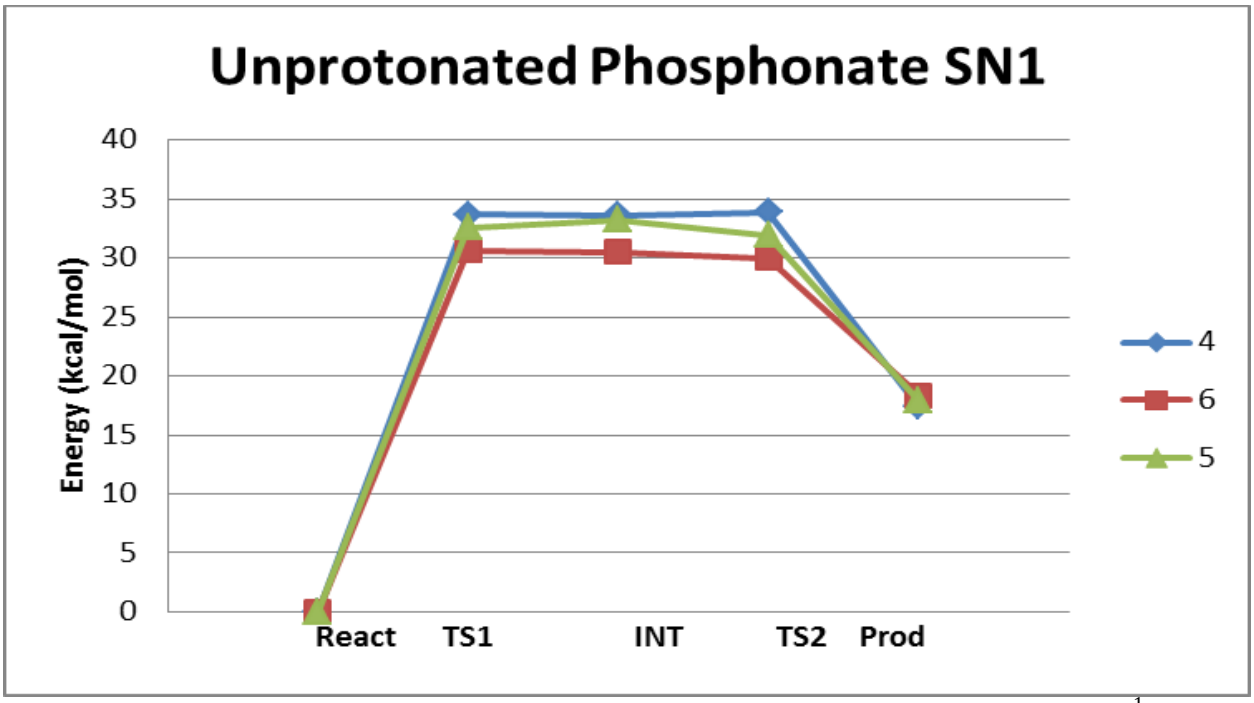

Figure B1: Reaction coordinate diagram for the S_N1 data of the unprotonated *ortho* QMPs.[1]

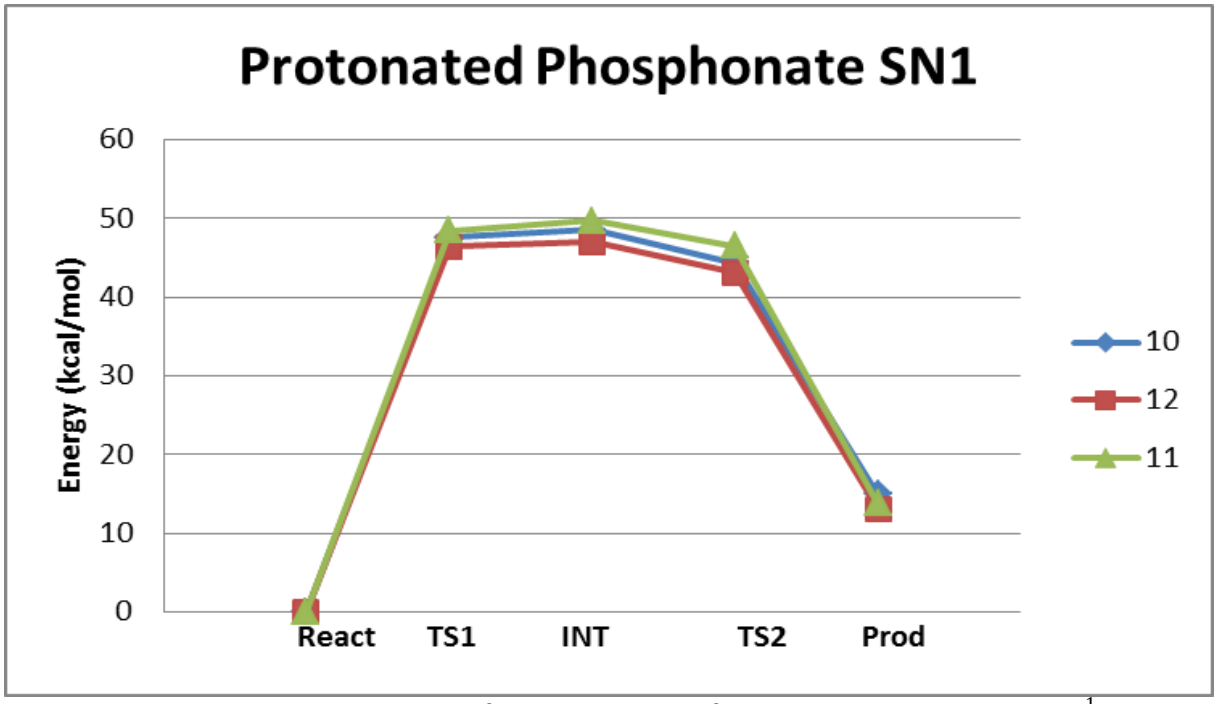

Figure B2: Reaction coordinate energies for the S_N1 data of the protonated *ortho* QMPs.[1]

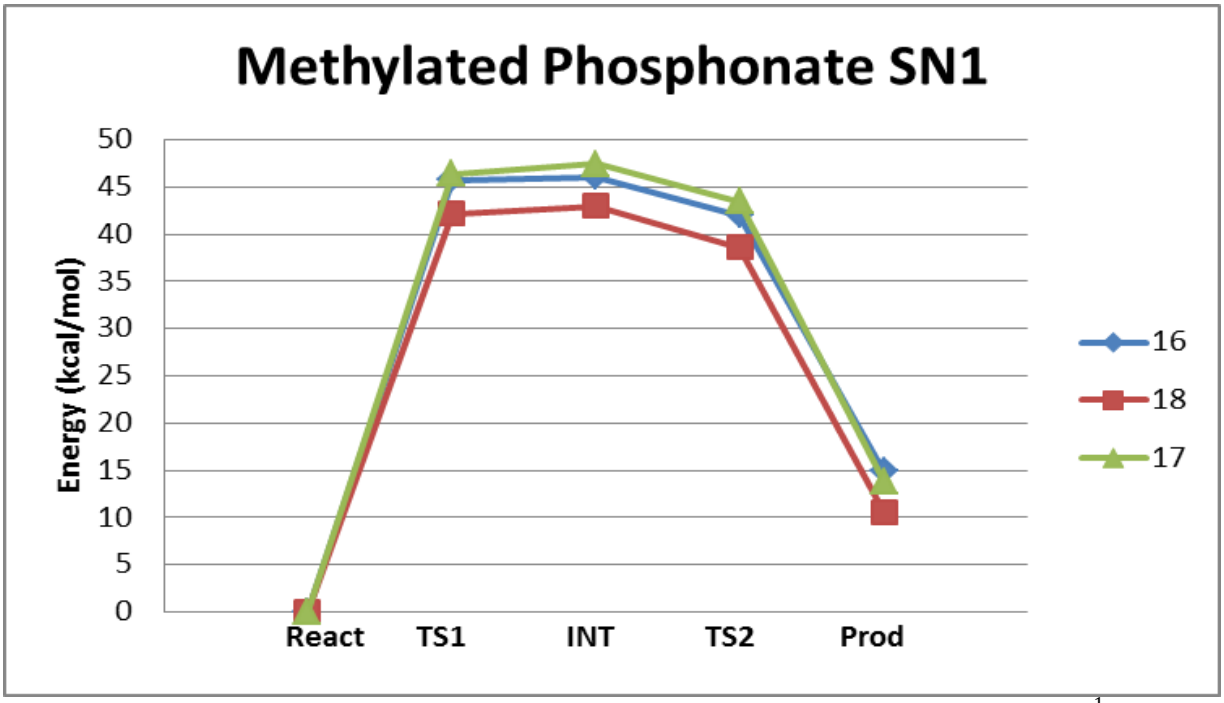

Figure B3: Reaction coordinate energies for the S_N1 data of the methylated *ortho* QMPs.[1]

Name	Reactant Energy (kcal/mol)	TS1 Energy (kcal/mol)	C-N Bond Length (Å)	Intermediate Energy (kcal/mol)	TS2 Energy (kcal/mol)	C-O Bond Length (Å)	Product Energy (kcal/mol)
p-mN-0-Me2H (**2**)	0.00	22.27	2.73	21.51	23.93	2.09	12.71
p-oN-0-Me2H (**1**)	0.00	22.00	2.85	21.84	23.61	2.09	13.17
o-m'N-0-Me2H (**3**)	0.00	25.48	2.70	25.43	27.03	2.10	13.04
p-mN-H-Me2H (**8**)	0.00	36.06	-	37.69	31.97	-	9.76
p-oN-H-Me2H (**7**)	0.00	42.25	-	43.78	39.61	-	11.48
o-m'N-H-Me2H (**9**)	0.00	35.14	-	36.98	32.56	-	12.39
p-mN-Me-Me2H (**14**)	0.00	33.46	-	34.88	30.14	-	9.39
p-oN-Me-Me2H (**13**)	0.00	40.11	-	41.73	37.86	-	11.09
o-m'N-Me-Me2H (**15**)	0.00	32.64	-	34.47	30.72	-	10.53

Table B2: Reaction coordinate energies for the S_N1 data of the *para* and *ortho-meta* prime QMPs. Energies are calculated relative to reactants. [2]

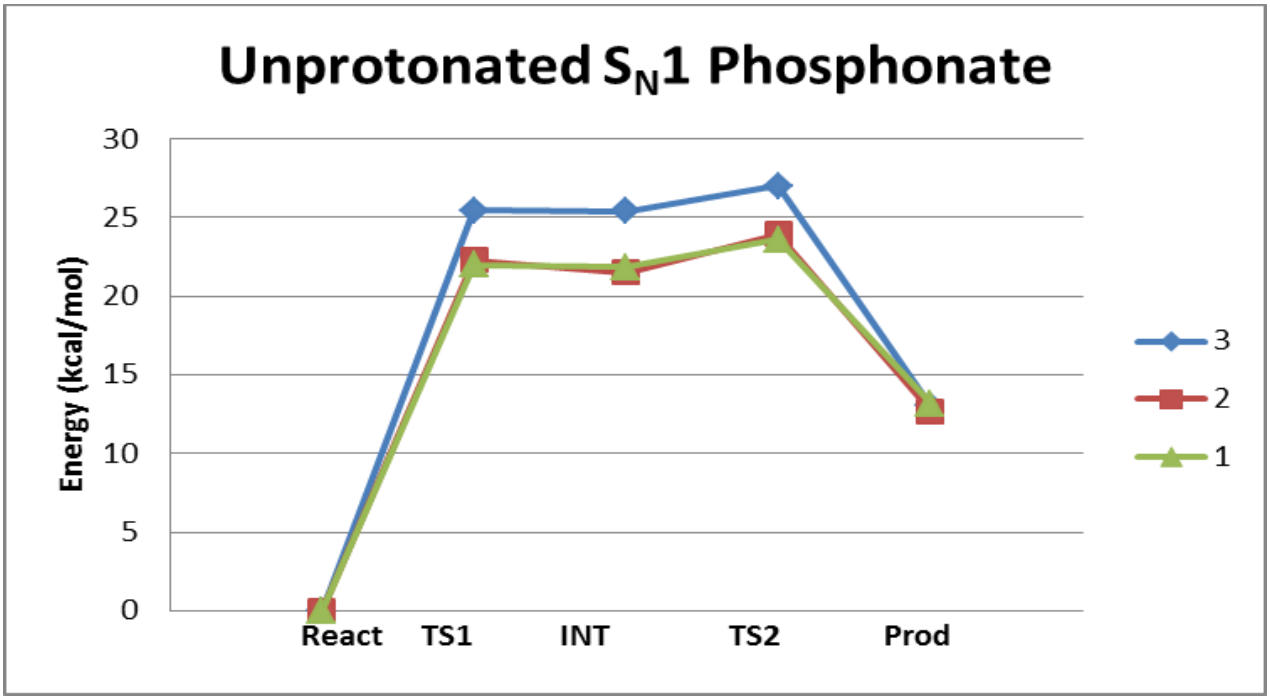

Figure B4: Reaction coordinate diagram for the S_N1 data of the unprotonated *para* and *ortho-meta* prime QMPs.[2]

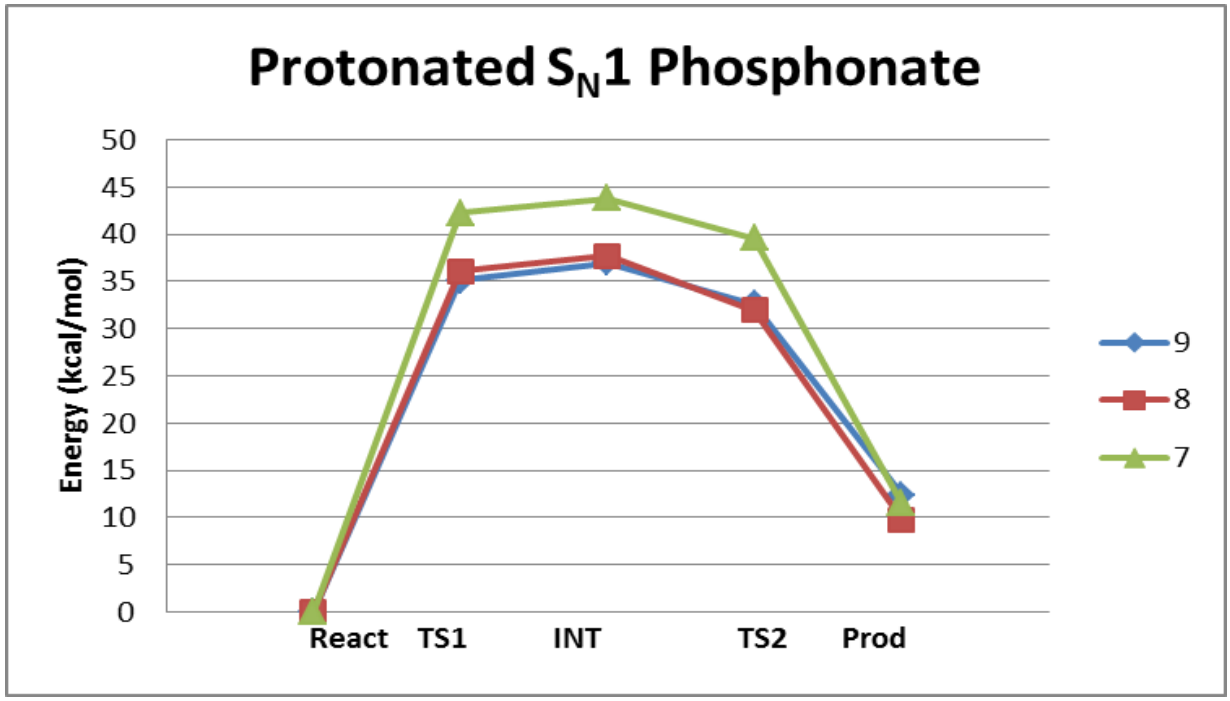

Figure B5: Reaction coordinate diagram for the S_N1 data of the protonated *para* and *ortho-meta* prime QMPs.[2]

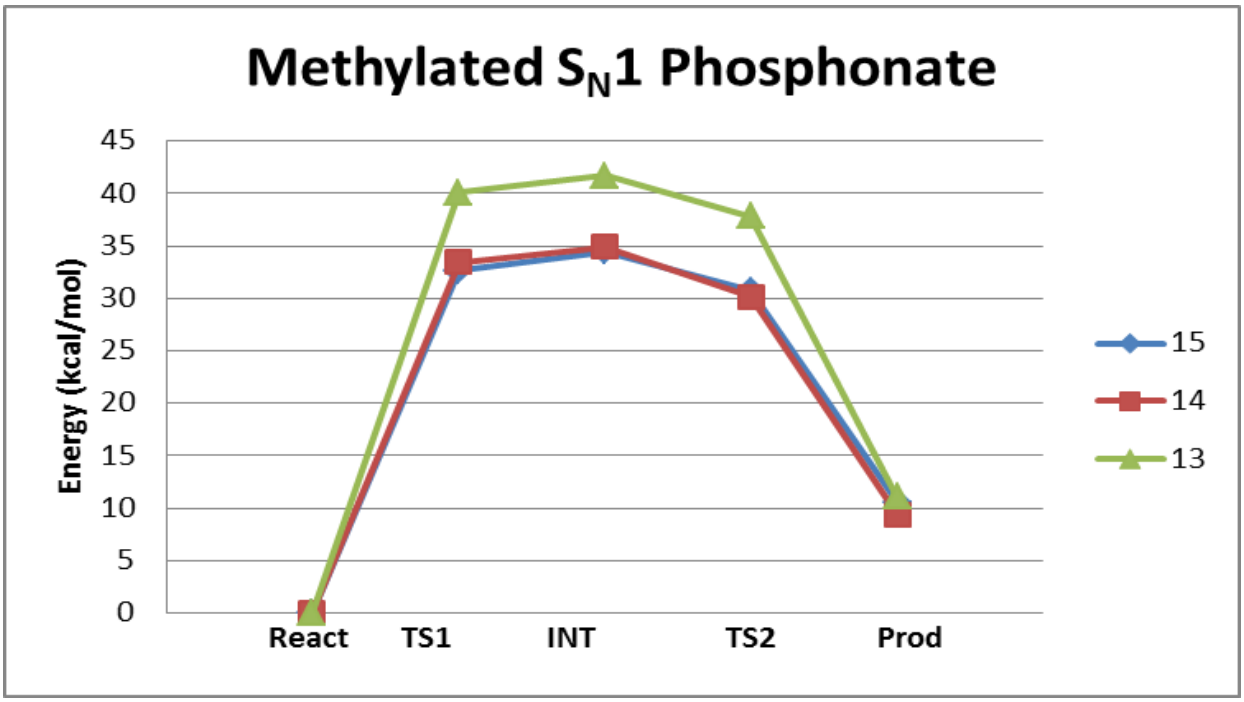

Figure B6: Reaction coordinate diagram for the S_N1 data of the methylated *para* and *ortho-meta* prime QMPs.[2]

S_N2 Data

Name	Reactant Energy (kcal/mol)	TS Energy (kcal/mol)	C-N Bond Length (Å)	C-O Bond Length (Å)	Product Energy (kcal/mol)
o-mN-0-Me2H (**4**)	-	-	-	-	-
o-oN-0-Me2H (**6**)	-	-	-	-	-
o-pN-0-Me2H (**5**)	-	-	-	-	-
o-mN-H-Me2H (**10**)	0.00	32.16	2.26	1.96	11.41
o-oN-H-Me2H (**12**)	0.00	36.97	2.28	1.97	17.19
o-pN-H-Me2H (**11**)	0.00	33.50	2.27	1.97	12.85
o-mN-Me-Me2H (**16**)	0.00	33.63	2.26	1.96	13.69
o-oN-Me-Me2H (**18**)	0.00	33.33	2.28	1.98	12.54
o-pN-Me-Me2H (**17**)	0.00	37.58	2.29	1.97	17.58

Table B3: Reaction coordinate energies for the S_N2 data of the *ortho* QMPs. Energies are calculated relative to reactants. [1]

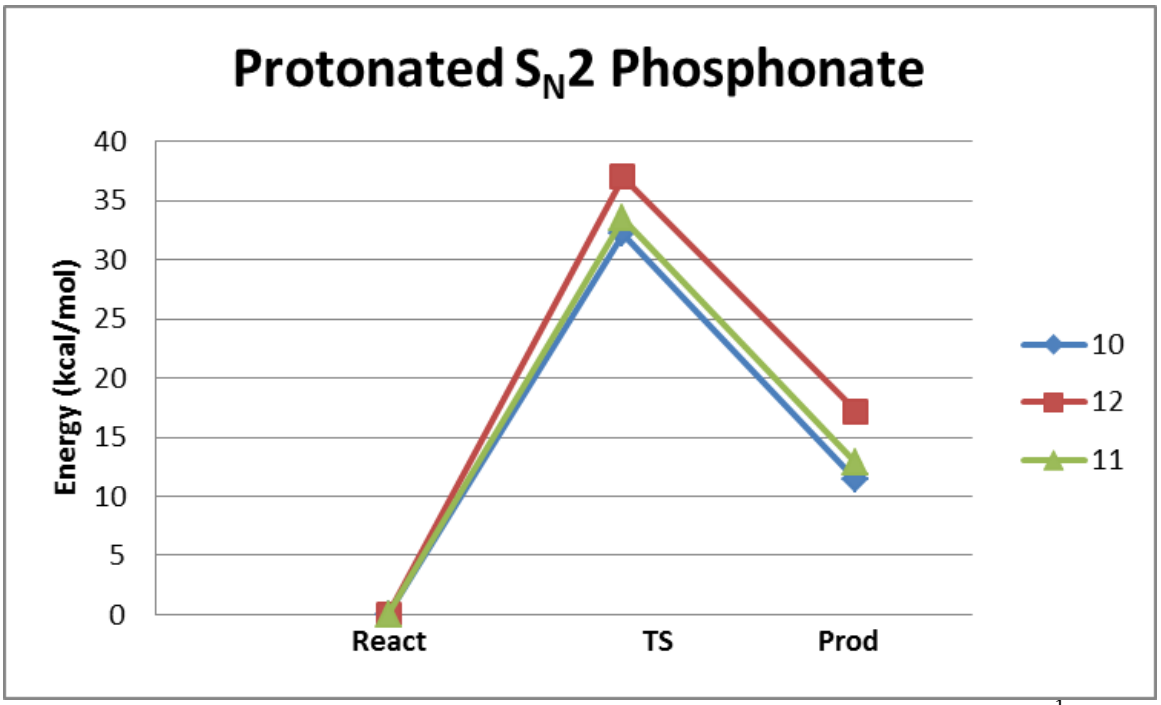

Figure B7: Reaction coordinate diagram for the S_N2 data of the protonated *ortho* QMPs.[1]

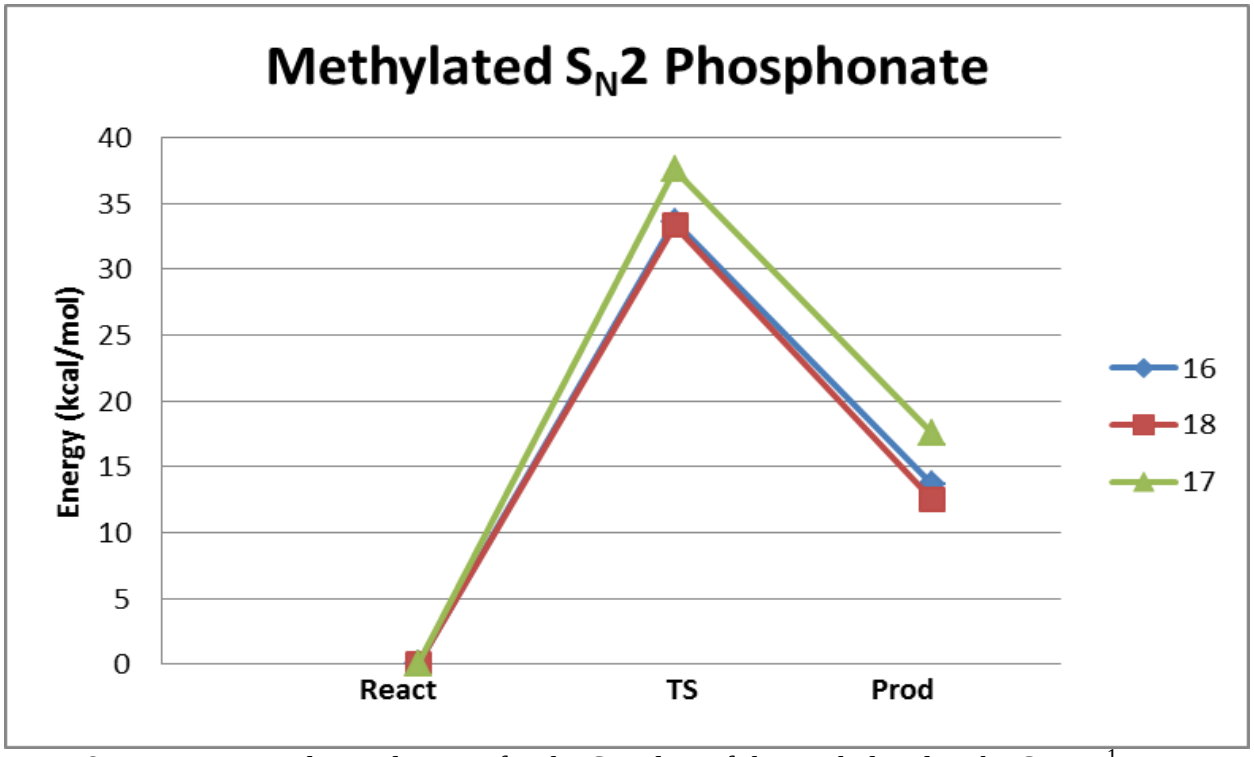

Figure B8: Reaction coordinate diagram for the S_N2 data of the methylated *ortho* QMPs.[1]

Name	Reactant Energy (kcal/mol)	TS Energy (kcal/mol)	C-N Bond Length (Å)	C-O Bond Length (Å)	Product Energy (kcal/mol)
p-mN-0-Me2H (**2**)	-	-	-	-	-
p-oN-0-Me2H (**1**)	-	-	-	-	-
o-m'N-0-Me2H (**3**)	-	-	-	-	-
p-mN-H-Me2H (**8**)	0.00	31.32	2.33	2.00	11.51
p-oN-H-Me2H (**7**)	0.00	33.98	2.32	1.98	14.74
o-m'N-H-Me2H (**9**)	0.00	44.71	2.32	1.99	22.35
p-mN-Me-Me2H (**14**)	0.00	30.27	2.41	2.05	10.65
p-oN-Me-Me2H (**13**)	0.00	33.30	2.29	1.98	12.16
o-m'N-Me-Me2H (**15**)	0.00	34.91	2.35	2.01	15.69

Table B4: Reaction coordinate energies for the S_N2 data of the *para* and *ortho-meta* prime QMPs. Energies are calculated relative to reactants. [2]

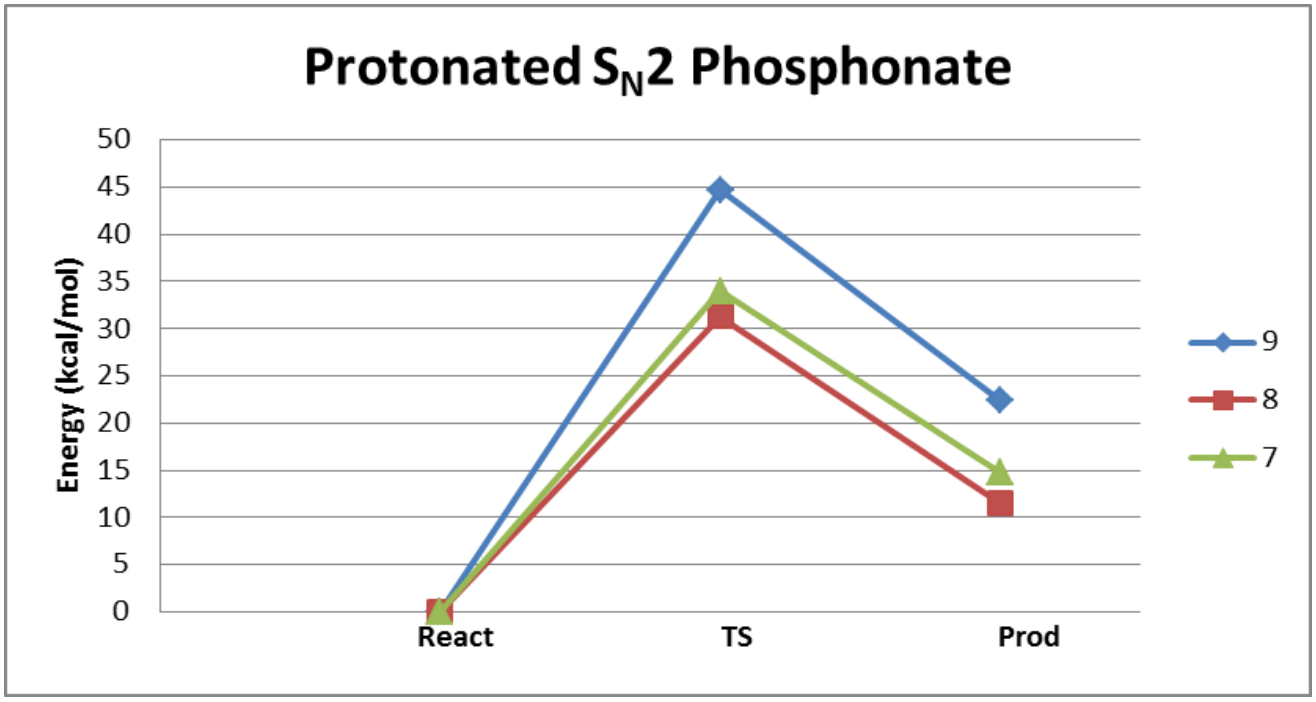

Figure B9: Reaction coordinate diagram for the S_N2 data of the protonated *para* and *ortho-meta* prime QMPs.[2]

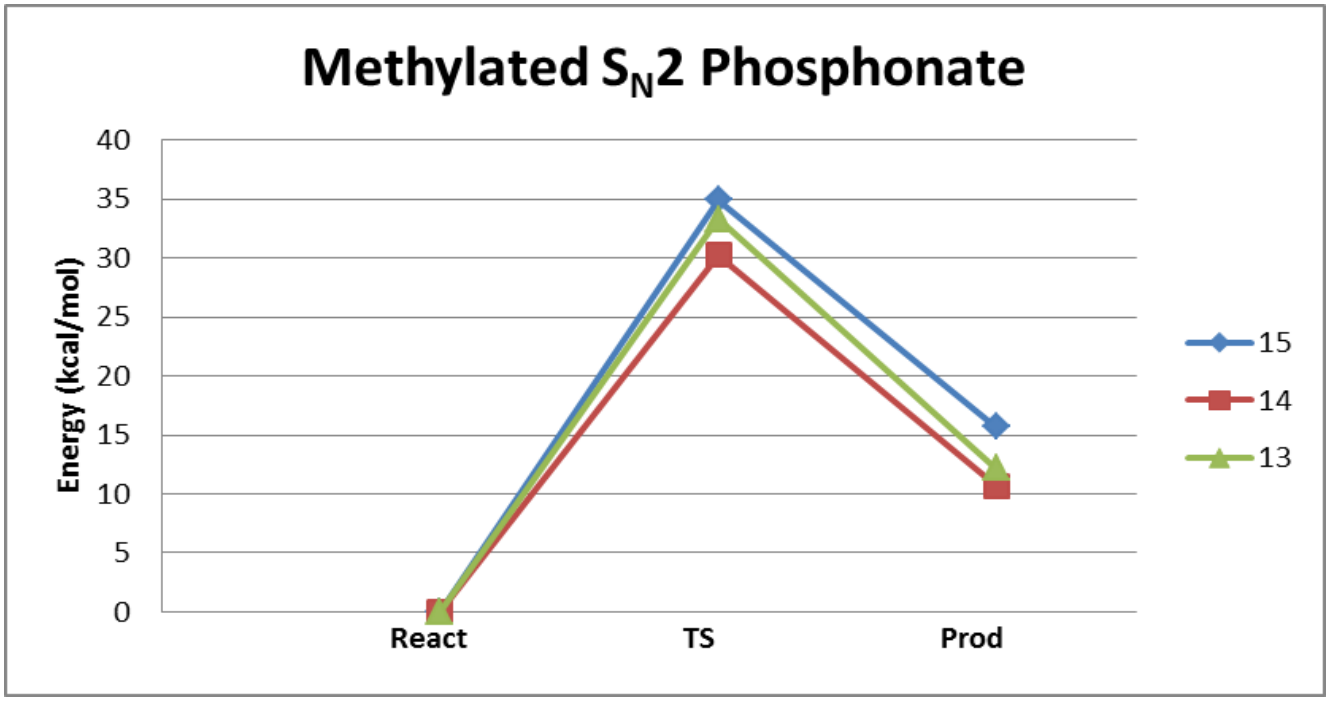

Figure B10: Reaction coordinate diagram for the S_N2 data of the methylated *para* and *ortho-meta* prime QMPs.[2]

[1]Indicates calculation performed by Andrew Franjesevic
[2]Indicates calculation performed by Keegan Fitzpatrick